


Particle filter-based prognostics for composite curing process

Aravind Balaji¹  | David Dumas¹ | Olivier Pierard¹ | Claudio Sbarufatti² | Francesco Cadini²

¹Cenaero Research Center, Charleroi, Belgium

²Department of Mechanical Engineering, Politecnico di Milano, Milan, Italy

Correspondence

Aravind Balaji, Cenaero Research Center, Rue des Frères Wright 29, 6041 Charleroi, Belgium.

Email: aravind.balaji@cenaero.be

Funding information

H2020 Marie Skłodowska-Curie Actions, Grant/Award Number: 859957

Abstract

Process-induced deformation (PID) arises in thermoset parts due to internal residual stress developed from their anisotropic properties, resulting in distortions. While passive numerical manufacturing control exists, active manufacturing control is crucial for enhancing the manufacturing process. The work focuses on diagnosing the polymerization reaction, known as the curing process, to consider the influence of uncertainties in thermal loading conditions on the behavior of cure kinetics. This is achieved using a Particle Filter approach, wherein a posterior distribution of cure evolution is recursively approximated based on observed measurements from characterization tests. The algorithm is designed to simultaneously perform the diagnosis and prognosis of the Degree of Cure and PID. This approach adopts the augmented cure formulation to address various scenarios with uncertainties in thermal loading conditions. It offers the advantage of providing comparable PID predictions with minimal computational costs. C-shaped thermoset parts made of epoxy/carbon fibers with varying thicknesses are cured using the Manufacturing Recommended Curing Cycle, and the predictions with the developed algorithm are validated against experimental measures. Upon validation, the converged prognosis capability of the Particle Filter model is employed to assess the impact of thermal loading uncertainty on cure profiles, which, in turn, affects the final PIDs outcome.

Highlights

- A Bayesian sampling approach enables the estimation of cure kinetics parameters.
- The estimated stochastic parameters forecast the process-induced deformations.

Abbreviations: CB, confidence boundary; CCS, coefficient of chemical shrinkage; CHILE, cure hardening linear instantaneous elastic (material model); CTE, coefficient of thermal expansion; DSC, differential scanning calorimetry; FE, finite element; FEA, finite element analysis; MC, Monte Carlo; MRCC, manufacturing recommended curing cycle; PDF, probability density function; PF, particle filter; PID, process-induced deformation; SIR, sequential importance resampling; SIS, sequential importance sampling.

This is an open access article under the terms of the [Creative Commons Attribution-NonCommercial](https://creativecommons.org/licenses/by-nc/4.0/) License, which permits use, distribution and reproduction in any medium, provided the original work is properly cited and is not used for commercial purposes.

© 2024 The Author(s). *Polymer Composites* published by Wiley Periodicals LLC on behalf of Society of Plastics Engineers.

- The augmented Degree of Cure accounts for uncertainties linked to thermal loadings.
- Analysis on AS4/8552 C-shaped parts shows the cure kinetics impact.
- The framework reduces the computational costs required for active control.

KEYWORDS

curing of polymers, differential scanning calorimetry (DSC), Monte Carlo simulation, processing

1 | INTRODUCTION

Thermoset composite materials have been extensively utilized in aerospace industries and necessitate numerous iterative analyses, covering material properties, mold characteristics, and more, before an efficient manufacturing process is established. This is primarily due to the occurrence of process-induced deformations (PIDs) observed during the manufacturing stage.^{1,2} Composite parts undergo distortion and develop internal residual stresses after being processed within the mold during the manufacturing phase, even in the absence of external forces and thermal gradients.^{3–5} Throughout the polymerization reaction, also known as the curing process, the thermoset resin transitions from a viscous state to a rubbery state and finally to a glassy state. During these transitions, the composite material undergoes deformations due to the thermal and chemical behavior of the resin.⁶ However, such deformations are constrained from occurring freely due to contact with the mold during the curing process. This leads to the development of internal residual stresses ranging from micro-scale to macro-scale.

Thermally induced stress fields are generated due to the discrepancy between the coefficients of thermal expansion (CTE) of the resin and the fibers.^{2,7} These thermal residual stresses are tensile in nature for the resin and compressive for the fiber. This is due to the considerably higher CTE of the resin compared to that of the fiber. Another source of residual stresses originates from chemical shrinkage, which is linked to the coefficients of chemical shrinkage (CCS). This phenomenon leads to a reduction in the free volume of the resin during the curing process. As the temperature rises, the resin molecules undergo end-linking reactions that draw them inwards, causing transitions between different states. Consequently, the available space within the resin decreases, exerting pressure on the fibers and generating internal residual stress that is uniformly distributed throughout the entire composite laminate. A diverse set of approaches is being employed to evaluate the internal residual stress in thermosetting composites.⁸ Upon demoulding, the stresses at the free surface are released,

causing the manufactured thermoset parts to assume distorted shapes.

From a macro-scale perspective, intrinsic factors such as composite orthotropic properties, stacking sequence, part thickness, mold material, and mold-part interaction have been found to exert a significant impact on PIDs.^{9–13} Furthermore, extrinsic factors come into play, such as thermal loading conditions and the mold properties used in the manufacturing process.¹⁴ It is essential to understand and account for both intrinsic and extrinsic influences to optimize the manufacturing process and ensure the desired product quality.

PIDs cause significant difficulties in the final assembly of composite structures, leading to increased costs.⁴ Moreover, they reduce the part's fatigue life and reliability.^{15,16} Additionally, design and assembly compensation strategies, such as shimming, unfortunately, result in an increase in residual stresses.⁵ Therefore, the approach of mold compensation is adopted, where the negative deformation prediction associated with the thermoset part is used to design the mold. The PIDs are represented in the form of warpage and spring-in/spring-out angles for flat and curved thermoset parts, respectively. The term 'spring-in' denotes a reduction in the desired angles, while 'spring-out' represents the opposite effect. Within the industry, trial-and-error methods associated with predicting PIDs prove to be expensive and time-consuming. Several analytical approaches^{17–21} have been introduced to predict the thermoelastic and non-thermoelastic components of volumetric free strains influencing the PIDs. These contributions have been observed to depend on the cure process variables and mechanical properties.²²

Alternatively, finite element analysis (FEA) coupled with mechanical constitutive models has been proven to be highly effective in predicting PIDs based on the shear-lag theory.²³ Various mechanical constitutive models, such as elasticity, pseudo-viscoelasticity, and viscoelasticity, have been implemented over the years.²⁴ Fully viscoelastic models,^{25–29} accurately portray curing behavior but require extensive material characterization and involve high computational costs.⁵ Meanwhile, the Cure Hardening Instantaneously Linear Elastic (CHILE) model establishes less

complex incremental elastic relations to describe changes in modulus as a function of cure process variables wherein a viscoelastic model based on path dependence on cure process variables is implemented.^{30–34} Although finite element (FE)-based constitutive models provide close predictions, gaining insights into the fundamental mechanisms controlling the PIDs is challenging due to the many assumptions involved. These assumptions involve disregarding the contact properties between plies and between the part and mold. Moreover, in thin laminate parts, the resin flow aspect is neglected. Additionally, numerical simulations involving complex thermoset parts with molds may encounter potential convergence issues. Such issues are predominantly associated with deviations in the mesh, particularly in curved sections. As a result, numerous improved analytical/semi-analytical expressions have been developed based on the shear-lag theory for curved thermoset parts.^{16,35} Such analytical expressions have been extended for more complex shapes, such as the L-shaped thermoset part, to account for the effect of the flange on PIDs, in addition to the curved sections of the part itself.^{36,37}

Given the uncertainties arising from many sources like the variation in the thermo-physical and thermo-mechanical properties, a deterministic cure model based analytical or numerical approach cannot yield satisfactory prediction results.³⁸ Therefore, there is compelling need for stochastic approaches. Studies in the literature underscore the importance of stochastic numerical simulations of cure temperature variation predictions to capture the uncertainty in curing processes.^{39–43} Furthermore, these variations in curing temperature cause uncertainty in the cure kinetics of thermoset materials. Such variability in the cure kinetics, affecting the PIDs, has received very limited attention in the literature. The previously discussed FE-based numerical and analytical models consider the parameters associated with cure kinetics to be deterministic. Consequently, they overlook the expected variability in cure process variables, specifically the Degree of Cure. In a recent study,⁴⁴ a stochastic cure simulation model using a Monte Carlo (MC) scheme is implemented to elucidate the impact of uncertainty in the cure kinetics model. Integrated thermo-mechanical FE models combined with Neural Networks while overlooking the cure process mechanisms, may suffice for swiftly predicting the PIDs.^{45–48} However, the demand for a significant volume of high-fidelity data and time-intensive training procedures makes it challenging. Moreover, the sensitivity of the influencing cure process parameters on the PIDs can be useful for optimizing the cure cycle.^{49–51} Consequently, there is a need for a systematic framework which allows the probabilistic

prediction of the PIDs while treating cure model parameters stochastically under thermal loading uncertainties.

A literature review on uncertainty analysis of thermoset manufacturing processes reveals significant limitations: The characterization of the cure process in thermoset materials is achieved using a parameterized diffusion cure-kinetics model that relies on controlled temperature. However, existing numerical and analytical models often treat the model parameters as deterministic, neglecting uncertainties arising from thermal loading conditions related to the part. Furthermore, the complexity intensifies with increasing part thickness or in the case of parts with curvatures, which are frequently associated with non-uniform polymerization as observed in the aerospace industry. Consequently, there is a growing need to incorporate stochastic treatment of the model parameters. Moreover, there is a compelling need for active manufacturing control, wherein the cure cycle would be automatically adjusted during processing based on real-time manufacturing data, such as part temperature and Degree of Cure. This approach would enable efficient manufacturing analysis, contrasting with the practice of assuming a range of convective thermal loading conditions through passive FE analyses, which are computationally demanding.^{52,53}

The objective of the study is to develop an active manufacturing control approach enabling multiple iterations of the PID predictions while accounting for a diverse array of thermal loading conditions. In this study, a stochastic framework tied to the volume of the thermoset part is proposed to consider the uncertainty related to the Degree of Cure, utilizing a diffusion cure-kinetics model.⁵⁴ A stochastic simulation approach is employed in the form of Particle Filters (PF), denoting a category of MC sampling techniques that utilize particle-based representations of Probability Density Functions (PDFs) in a sequential manner, characterized by a state-space model.^{55,56} The methodology incorporates Sequential Importance Sampling/Resampling (SIS/SIR) procedures^{57,58} to preserve uncertainties associated with the phenomenon described by diffusion cure-kinetics model and experimental differential scanning calorimetry (DSC) measurements. The correlation between the Degree of Cure of a thermoset part and the measurements exhibits variations due to uncertainties in manufacturing conditions and autoclave tolerances. In this work, we utilize the SIR PF algorithm to represent the uncertainty associated with the evolution of the Degree of Cure, as described by the diffusion cure-kinetics model, while also accounting for the inherent randomness in the curing process. The filtered information serves as the basis for updating the PDFs of future Degree of Cure evolutions. Furthermore, the model parameters related to the cure are incorporated

into the state vectors, and their corresponding PDFs are progressively updated using DSC measures. The parameters, treated stochastically at discrete time steps, are employed for predicting forthcoming Degree of Cure and final PIDs. The PIDs are generated using an analytical solution with a generalized plane strain assumption, considering three-dimensional effects on the spring-in of curved composite parts. This considers both the volumetric free strain generated during the curing process in the through-thickness direction and in the length direction.³⁵

The development of volumetric free strain is observed to depend on the evolution of the Degree of Cure. Given the assumptions that (A) material properties remain constant both before and after cure transition points, and (B) there is a sudden change in material properties upon cure transitions, the evaluation of the Degree of Cure informs the occurrence of cure transition points during manufacturing. The updated information on model parameters is employed to update the PDFs of the transition points at discrete time steps. The forecasting of final PIDs, contingent on cure transition points, becomes particularly valuable in scenarios involving thermal loading condition uncertainty.

2 | EXPERIMENTAL

2.1 | Cure process associated variables

The crucial variables pertinent to the cure process include the Degree of Cure, x , the glass transition temperature, T_g , volumetric free strains, CTEs and CCSs. The variable x is the ratio between the heat released at time t and the total amount of heat released during curing process, ranging between zero (representing a fully uncured resin) and one (indicating a fully cured resin). Note that it is considered as the system state to be estimated. The Degree of Cure delineates the system's state throughout the curing process, representing the fraction of heat released at a given time relative to the total heat liberated during the entire curing procedure.

The critical points in the Degree of Cure evolution are the gelation and vitrification points, which define the transition between viscous and rubbery states and between rubbery and glassy states, respectively. The gelation point is considered a transition point during the cure cycle at which the resin is capable of sustaining mechanical loads. Upon transitioning into the glassy state within the curing process, there is a notable reduction in molecular mobility due to the diminished resin volume. This phenomenon is quantified by the T_g . The vitrification is understood to occur when the cure temperature, T matches with the, T_g which is described to be dependent on x . This relationship is described by DiBenedetto's

relationship.⁵⁹ Moreover, the material properties are anisotropic and vary in different states of cure. The thermo-material properties, especially the CTE and CCS are very much dependent on Degree of Cure, given by,

$$\alpha | \beta = \begin{cases} \alpha^v | \beta^v \forall x < x_{\text{gel}} \text{ and } x < x_{\text{vitr}} \\ \alpha^r | \beta^r \forall x \geq x_{\text{gel}} \text{ and } x < x_{\text{vitr}} , \\ \alpha^g | \beta^g \forall x > x_{\text{vitr}} \end{cases} \quad (1)$$

where α^i and β^i represent the CTEs and CCSs in various states throughout the cure process, respectively. The superscripts, v , r , and g represents the viscous, rubbery and glassy states respectively. The shift in such thermo-material properties drives the computation of volumetric free strain, ϵ , in different states given by,

$$\begin{cases} \epsilon^v = \int_{t_{\text{initial}}}^{t_{\text{gel}}} \alpha^v \left(\frac{\partial T}{\partial t} \right) dt + \int_{t_{\text{initial}}}^{t_{\text{gel}}} \beta^v \left(\frac{\partial x}{\partial t} \right) dt \\ \epsilon^r = \int_{t_{\text{gel}}}^{t_{\text{vitr}}} \alpha^r \left(\frac{\partial T}{\partial t} \right) dt + \int_{t_{\text{gel}}}^{t_{\text{vitr}}} \beta^r \left(\frac{\partial x}{\partial t} \right) dt , \\ \epsilon^g = \int_{t_{\text{vitr}}}^{t_{\text{final}}} \alpha^g \left(\frac{\partial T}{\partial t} \right) dt + \int_{t_{\text{vitr}}}^{t_{\text{final}}} \beta^g \left(\frac{\partial x}{\partial t} \right) dt \end{cases} \quad (2)$$

where t_{gel} and t_{vitr} represent the time corresponding to the occurrence of gelation and vitrification phenomena, respectively. The first and second terms in Equation (2) correspond to the thermoelastic and non-thermoelastic components, respectively. The thermoelastic component relates to the thermal expansion of the composite, while the non-thermoelastic component pertains to effects associated with chemical shrinkage and the interaction between the mold and the part. It is assumed that there is sufficient stress build-up in the viscous state, and the volumetric free strains are considered insignificant. Upon gelation, a reduction in free volume within the resin, caused by chemical shrinkage, is coupled with matrix expansion due to thermal expansion. Additionally, upon entering the glassy state, the impact of chemical shrinkage diminishes. Note that the thermal effect is not considered when the isothermal temperature remains stable, while it is during the cooling phase of the curing cycle. These volumetric free strains remain to be the primary cause of PIDs.⁶⁰

2.2 | Experimental DSC analysis

The DSC test is conducted to provide the rate of Degree of Cure for a specific temperature curing cycle, denoted as $\frac{dx}{dt}$. This test involves measuring the heat flow difference between capsules containing the resin sample under analysis and a reference resin sample.

The materials of interest are the unidirectional AS4/8552 prepregs produced by Hexcel.⁶¹ A 5-milligram sample of unidirectional AS4/8552 prepreg is subjected to a curing cycle, and the variables corresponding to exothermic and endothermic phenomena are recorded. During the initial stages of the curing process, the $\frac{dx}{dt}$ is relatively slow because of the presence of unreacted functional groups within the resin. As the curing process advances, the quantity of these unreacted functional groups decreases, resulting in an acceleration of the $\frac{dx}{dt}$. The onset of this acceleration marks the gelation point, t_{gel} . Eventually, the $\frac{dx}{dt}$ slows down again as the resin approaches the cure threshold. This value refers to a critical level of polymerization beyond which the mechanical properties remain virtually unchanged.

Three DSC experiments, each with two repetitions corresponding to temperature cycles at three different rates (1.5, 0.55, and 0.5°C/min) with isothermal dwells at 180, 175, and 185°C, respectively, are conducted, as shown in Figure 1. Two DSC experiments, each with two repetitions corresponding to partial cure cycles, are conducted, in addition. For the partial curing cycle 1, it involves an initial heating ramp from room temperature to 107°C at a rate of 0.50°C/min, followed by a hold at 107°C for 30 min. Then, there is a rise to 144°C at 0.50°C/min, followed by a return to room temperature by quenching at 10°C/min. Subsequently, there is another rise from room temperature to 153°C at 2.5°C/min, followed by a rise from 153 to 180°C at a rate of 0.50°C/min, maintaining 180°C for 210 min. Meanwhile for the case of partial curing cycle 2, it entails a rise from room temperature to 143°C at a rate of 0.5°C/min, followed by a return to room temperature by quenching at 1.5°C/min. Then, there is a subsequent rise from room temperature to 153°C at 2.5°C/min, followed by a rise from 153 to 180°C at a rate of 0.50°C/min. The material is then held at 180°C for 210 min after which it is cooled down to room temperature at 1.5°C/min. The temperature for all the DSC tests is gradually reduced to room temperature at a rate of 1.5°C/min.

Dynamic Mechanical Analysis, in combination with DSC tests helps in assessing the cure threshold value, which, on average, from the characterization tests, correspond to 0.93. The onset of gelation for the DSC tests is found to occur at 0.21. Moreover, the glass transition temperature, T_g , which determines the transition from the rubbery to the glassy state, is correlated with x in the set of DSC experiments with the following relation,

$$T_g = (39.908x^2) + (222.369x) - 32.172. \quad (3)$$

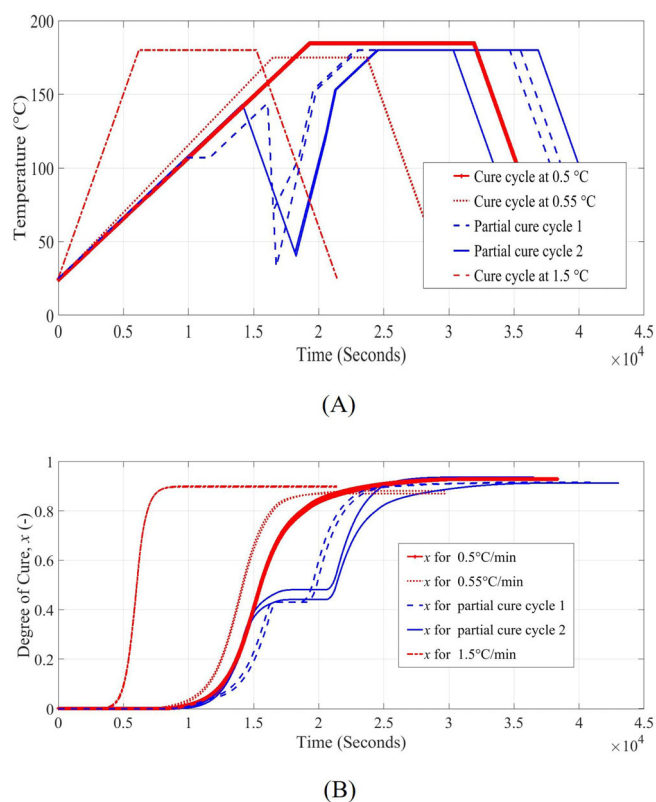


FIGURE 1 (A) Differential scanning calorimetry characterization tests under different thermal loading conditions, illustrating. (B) The evolution of the Degree of Cure.

This relation is implemented to find the transition point, t_{vitr} corresponding to the vitrification phenomenon (i.e., when $T = T_g$) within the study. Note that with the partial cure cycles, the cure kinetics enable achieving gelation during the first return to room temperature and then restarting the Degree of Cure evolution as soon as 153°C is reached during further increments in the temperature cycle. Consecutively, the occurrence of the vitrification point is significantly delayed. The DSC characterization tests corresponding to different cycles shows the potential for modifying the polymer cure kinetics morphology is significant, and a physical cure kinetic model with deterministic parameters alone cannot suffice for such cases.

3 | PARTICLE FILTER-BASED PROGNOSTIC FRAMEWORK

3.1 | Degree of cure modeling

Consider that a discrete representation of a cure evolution model can be described as.

$$x_k = f(x_{k-1}, \mathbf{\Omega}), \quad (4)$$

where $\mathbf{\Omega}$ is a vector encompassing the parameters that govern the curing evolution, and the subscript k denotes the k^{th} discrete time step. The function $f(\cdot)$ typically describes a physical cure-kinetics model. The parameters $\mathbf{\Omega}$ vary across various states throughout the curing process, attributed to uncertainties in the cure associated with temperature variations. Within the study,⁷ a diffusion cure-kinetics model with different constants is recommended for temperature rates below 3°C/min. With discrete time steps, the diffusion cure-kinetics model,⁵⁴ is discretized, and the value of x in next time step k is given by:

$$x_k = f(x_{k-1}, \mathbf{\Omega}) = x_{k-1} + e^{\tau_k} \left[\frac{Ae^{-Q/R_u T} x_{k-1}^m (1 - x_{k-1})^n}{1 + e^{c(x_{k-1} - (\kappa_0 - (\kappa_t T)))}} \right], \quad (5)$$

where R_u represents the universal gas constant, A stands for the pre-exponential cure coefficient, Q denotes the activation energy, while m and n correspond to the first and second exponents. Additionally, c is the diffusion constant, κ_0 signifies the critical Degree of Cure at the beginning, and κ_t is a constant that factors in the influence of x as the temperature changes. $\tau_k \sim \mathcal{N}\left(-\frac{\sigma_k}{2}, \sigma_{\tau_k}^2\right)$ represents non-zero normally distributed Gaussian noise, adding intrinsic stochastic characteristics to the cure evolution. The vector, $\mathbf{\Omega} = [A; Q; m; n; c; \kappa_0; \kappa_t]$ corresponds to the diffusion cure-kinetics parameters.

Consideration of a deterministic model may hardly yield precise transitions in the Degree of Cure, which are ultimately crucial for accurately modeling the volumetric free strains contributing to PIDs induced by the curing process. By resorting to a common practice in PF-based prognosis,⁵⁸ the parameters $\mathbf{\Omega}$ are considered as stochastic variables updated within the process equation given by,

$$\mathbf{z}_k = \begin{bmatrix} \mathbf{\Omega}_k \\ x_k \end{bmatrix} = \begin{bmatrix} \mathbf{\Omega}_k + \tau_{\Omega, k} \\ f(x_{k-1}, \mathbf{\Omega}_k, \tau_k) \end{bmatrix}, \quad (6)$$

where \mathbf{z} represents the cure process vector, including both the Degree of Cure x and the diffusion cure-kinetics parameters $\mathbf{\Omega}$. Meanwhile, τ and τ_{Ω} represent the noises for the Degree of Cure and the cure-kinetics parameters, respectively. Due to challenges in directly measuring the cure process variables, we infer the unknown Degree of Cure from indirect DSC experimental measurements denoted as y , which are interconnected through a measurement equation $g(\cdot)$. The formulation of the cure prognosis can be expressed as follows,

$$\begin{cases} \mathbf{z}_k = \begin{bmatrix} \mathbf{\Omega}_k \\ x_k \end{bmatrix} = \begin{bmatrix} \mathbf{\Omega}_k + \tau_{\Omega, k} \\ f(x_{k-1}, \mathbf{\Omega}_k, \tau_k) \end{bmatrix}, \\ y_k = g(x_k) + \omega_k \end{cases}, \quad (7)$$

where the function $g(\cdot)$ describes the relationship between the Degree of Cure x and the measurements y (i.e., the DSC measurements), and ω is a vector of measurement noise, assumed to be zero-mean Gaussian in this study.

3.2 | Particle filter

When a Bayesian approach is applied to the prognostic model, the unknown state vector, \mathbf{z}_k can be inferred from the measurement as follows,

$$p(\mathbf{z}_k | \mathbf{y}_{1:k-1}) = \int p(\mathbf{z}_k | \mathbf{z}_{k-1}) p(\mathbf{z}_{k-1} | \mathbf{y}_{1:k-1}) d\mathbf{z}_{k-1}, \quad (8)$$

$$p(\mathbf{z}_k | \mathbf{y}_{1:k}) \propto p(\mathbf{y}_k | \mathbf{z}_k) p(\mathbf{z}_k | \mathbf{y}_{1:k-1}), \quad (9)$$

where $\mathbf{y}_{1:k}$ is the measurement vector up to time step, k , the symbol \propto indicates the proportionality, the transition distribution $p(\mathbf{z}_k | \mathbf{z}_{k-1})$ and the likelihood function $p(\mathbf{z}_k | \mathbf{y}_{1:k-1})$ denote the diffusion cure-kinetics and measurement equations, respectively. Meanwhile, $p(\mathbf{z}_k | \mathbf{y}_{1:k-1})$ and $p(\mathbf{z}_k | \mathbf{y}_{1:k})$ are the prior and posterior-updated PDF of the augmented Degree of Cure vector, respectively. The estimation of the posterior PDF is conceptual and complicated to implement analytically. For this purpose, the SIR PF methodology is implemented to approximate the Bayesian solution for $p(\mathbf{z}_k | \mathbf{y}_{1:k})$.^{55,56} Table 1 lists the pseudo-code of SIR PF.

3.3 | Future degree of cure and PID prediction

Within a PF-based prognostic framework, the prognostic step enables the prediction of future Degree of Cure through the diffusion cure-kinetics model, based on the particles filtered with updated knowledge of the current Degree of Cure. The prediction for each particle stops when the future state reaches a pre-defined cure threshold value, corresponding to the final Degree of Cure. With the trajectories of the Degree of Cure, the transition points (i.e., gelation and vitrification points) are determined to compute the volumetric free strains, refer Equations (1) and (2) in Section 2.1 at the end of the cure process. Then, the PIDs are deemed to be a function of the volumetric free strain on basis of the deformation mechanism-based methods,^{35,62} denoted by $h(\cdot)$. The

function $h(\cdot)$, is detailed in Section 4.3 for the specific case of C-shaped thermoset laminates within the study. The procedure is outlined by the pseudo-code in Table 2.

4 | PARTICLE-FILTER MODEL IMPLEMENTATION

4.1 | Model formulation

The Degree of Cure evolution is highly dependent on the parameters mentioned in Section 3.1. Given the uncertainties arising from various thermal loading conditions, the parameters can be different for a different specimen.⁶³ The determination of the cure model parameters follows by fitting each experimental DSC curve defined in Section 2.2 to the diffusion cure-kinetics model. This procedure estimates the mean and standard deviation of each parameter. However, this procedure can potentially be influenced by the non-linearity of the Degree of Cure and the interdependencies of cure model parameters. The results of estimated model parameters from the DSC experiments through this outlined process are presented in Table 3.

To assess parameter sensitivity, we employ the diffusion cure-kinetics model, refer Equation (5). This involves varying each parameter by both one positive standard deviation and one negative standard deviation. For the case of testing, the sample subjected to the Manufacture Recommended Curing Cycle (MRCC) is studied.⁷ The MRCC is applied which consists of an initial increase of temperature with 2°C/min up to 120°C followed by an isothermal hold for 60 min. Then, a second increase of temperature with 2°C/min up to 180°C followed by another isothermal hold for 120 min. Finally, the temperature is brought back to room temperature with a 2°C/min rate.⁶¹ Subsequently, the average relative differences

TABLE 1 Sampling importance resampling particle filter procedure at time step k .

Initialization: Draw N_s particles $\{\mathbf{z}_0^i : i = 1, 2, \dots, N_s\}$ from the initial distribution $p(\mathbf{z}_0)$

For $i = 1, 2, \dots, N_s$

Prediction in PF: draw N_s particles $\{\mathbf{z}_k^i : i = 1, 2, \dots, N_s\}$ by $p(\mathbf{z}_k | \mathbf{z}_{k-1}^i)$

Weight update: calculate the weight w_k^i by $w_k^i \propto p(y_k | \mathbf{z}_k^i)$, and assign its normalized form, \tilde{w}_k^i to each particle \mathbf{z}_k^i

Resample for $\{\mathbf{z}_k^i : i = 1, 2, \dots, N_s\}$ using the particle weights $\{\tilde{w}_k^i : i = 1, 2, \dots, N_s\}$

End

in predicted Degree of Cure, x , with true measures at MRCC based on the estimated parameter values, were calculated. The resulting mean between these two values served as an indicator of the model's sensitivity to the variability of each parameter. The relative difference corresponds to increments equivalent to one standard deviation around the mean.

The highest discrepancies in the Degree of Cure, x , arise from Q and m , with relative differences of 12% and 13%, respectively. When considering a modification in the thermal loading condition of the cure cycle, accurate prediction of the future Degree of Cure and cure transition points through Equation (5) becomes challenging, especially when treating Q and m as deterministic and known. Both model parameters significantly influence the height and position of the $\frac{dx}{dt}$ and are treated as stochastic variables, $\Omega^{\text{sto}} = [Q; m]$, while the remaining model parameters are considered deterministic, $\Omega^{\text{det}} = [A; n; c; \kappa_0; \kappa_1]$, with the estimated value. The uncorrelated stochastic parameters, Ω^{sto} , are updated at every time step, forming the process equation within the PF framework is in the following form:

$$\begin{bmatrix} Q_k \\ m_k \\ x_k \end{bmatrix} = \begin{bmatrix} Q_{k-1} + \tau_{1,k} \\ m_{k-1} + \tau_{2,k} \\ x_{k-1} + e^{\tau_k} \left[\frac{Ae^{-Q_k/R_u T} x^{m_k} (1-x)^n}{1 + e^{\epsilon(x - (\kappa_0 - (\kappa_1 T)))}} \right] \end{bmatrix}, \quad (10)$$

where τ_1 and τ_2 represents the zero mean Gaussian process noises. The prediction of the future Degree of Cure clearly depends on the stochastic parameter estimation.

TABLE 2 Calculation of future Degree of Cure and final cure induced Process-induced deformation (PID) at time step k .

Initialization: Define samples of the Degree of Cure and evolution parameters from $\{\mathbf{z}_{\text{best},k}^i : i = 1, 2, \dots, N_s\}$ as $\{x_k^{i,0} : i = 1, 2, \dots, N_s\}$ and $\{\Omega_{\text{best},k}^i : i = 1, 2, \dots, N_s\}$, respectively

For $i = 1: N_s$

$l = 0$

While $x_k^{i,l} < \text{cure threshold}$

Calculate the future Degree of Cure, $x_k^{i,l+1}$

by $x_k^{i,l+1} = f(x_k^{i,l}, \Omega_{\text{best},k}^i)$

$l = l + 1$

End

Find Degree of Cure transition points (i.e., t_{gel}^i and t_{vitr}^i), refer to Equation (3)

Calculate volumetric free strains, e_k^i , refer to Equations (1) and (2)

Predict PID, $\text{PID}_k^i = h(e_k^i)$, refer to Section 4.3

End

Model parameters	Value	Std.	Relative difference in x (%)
A (s^{-1})	68,229	1.252×10^3	0.593
Q (J/mol)	64,240	1.209×10^3	12.120
m (-)	0.482	0.058	13.150
n (-)	1.750	0.005	0.026
C (-)	30.082	0.179	0.005
κ_0 (K^{-1})	5.261×10^{-3}	6.399×10^{-3}	0.003
κ_t (-)	-1.555	0.028	0.001

TABLE 3 Estimated kinetics parameters, standard deviation of kinetics parameters and sensitivity analysis results.

For this purpose, the method of kernel smoothing,⁶⁴ is adopted to improve the estimation of cure-kinetics constants. The stochastic parameter estimation using this technique is as follows,

$$\begin{cases} Q_k = \sqrt[2]{1-h^2} Q_{k-1} + (1 - \sqrt[2]{1-h^2}) \hat{Q} + \tau_{1,k} \\ m_k = \sqrt[2]{1-h^2} m_{k-1} + (1 - \sqrt[2]{1-h^2}) \hat{m} + \tau_{2,k} \end{cases}, \quad (11)$$

where \hat{Q} and \hat{m} represents the mean of samples for Q and m , and $h \in [0,1]$ is the kernel smoothing constant. By combining Equation (10) and Equation (11), the PF framework for the prediction of Degree of Cure is obtained as,

$$\begin{cases} \begin{bmatrix} Q_k \\ m_k \\ x_k \end{bmatrix} = \begin{bmatrix} \sqrt[2]{1-h^2} Q_{k-1} + (1 - \sqrt[2]{1-h^2}) \hat{Q} + \tau_{1,k} \\ \sqrt[2]{1-h^2} m_{k-1} + (1 - \sqrt[2]{1-h^2}) \hat{m} + \tau_{2,k} \\ x_{k-1} + e^{\tau_k} \left[\frac{A e^{-Q_k/R_u T} x_k^{m_k} (1-x)^n}{1 + e^{c(x - (\kappa_0 - (\kappa_t T)))}} \right] \end{bmatrix}, \\ y_k = g(x_k) + \omega_k \end{cases}, \quad (12)$$

where the measurements y is the Degree of Cure measures attained from the DSC test and the function $g(x_k)$ simply is the DSC cure measures at MRCC.⁷ Finally, the cure threshold, determined through the average of the DSC tests, is set at 0.93.

4.2 | Particle filter parameters

The parameter state estimation and the prognosis of the Degree of Cure within the PF framework rely on the proper tuning of the initial distribution and PF parameters. The selection of these values is crucial and has a profound influence on stochastic simulations. The initial Ω distribution is considered as

multivariate Gaussian. The Ω^{sto} in terms of a joint PDF with mean and covariance matrices, as defined by the statistical properties of diffusion cure-kinetics described in Table 3, is given as follows,

$$\mu[\Omega_{k=0}^{\text{sto}}] = \begin{bmatrix} 64240 \\ 0.482 \end{bmatrix}; \Sigma[\Omega_{k=0}^{\text{sto}}] = \begin{bmatrix} 1209 & -0.288 \\ -0.288 & 0.058 \end{bmatrix}. \quad (13)$$

The PDF assumes that Q and m are weakly correlated; that is, the covariance between the parameters has been set to -0.288 based on experimental DSC characterization tests in Section 2.2. Strong correlation can be particularly useful when significant differences exist corresponding to the $\frac{dx}{dt}$ peaks in repeated DSC tests due to uncertainties in thermal loading conditions. These correlations have an impact on the parameter state estimations during the sequential updating process in the PF algorithm.

A random multiplicative term, τ , is defined as $\mathcal{N}\left(-\frac{(1.250)^2}{2}, (1.250)^2\right)$, in the process equation using a trial-and-error approach to describe the evolution of the Degree of Cure with some perturbations to exploit its uncertainty. The log-normal distribution for the cure process noise ensures that the noise is consistently positive, with the mean value of Degree of Cure distribution dictated by its parameters. Non-zero Gaussian noises, $\tau_1 = \mathcal{N}(0, 100^2)$ and $\tau_2 = \mathcal{N}(0, 0.001^2)$ are defined based on repeated DSC tests at same thermal loading conditions. At every time step k , the process noise distributions are sampled and assigned to the particles. For the case of measurement noise, a zero-mean Gaussian distribution, $\omega = \mathcal{N}(0, 0.1^2)$ is chosen for the likelihood which is expressed as follows:

$$p(y_k | z_k^i) = \frac{1}{\sqrt{2\pi\sigma_{\omega_y}}} e^{\left(-\frac{1}{2\sigma_{\omega_y}^2} (y_k - y_k^i)^2\right)}, \quad (14)$$

where y_k is the measure at the k th discrete time step, y_k^i is the simulated observation for the state particle x_k^i and σ_{ω_y}

is the standard deviation of the measurement noise. The standard deviation for such a distribution is determined through a trial-and-error procedure, considering the error associated with the repeatability of DSC tests.⁶³ The choice of the number of particles should be made based on the specific requirements of the application, considering both the desired level of accuracy and the available computational resources. In this case, N_s is taken as 8000. Finally, the value of the kernel smoothing parameter, h from Equation (12) is set to 0.1 to maintain sample variety.

4.3 | PID prognostics and validation

The selected thickness for the analyses of PID within this study ranges from 2 to 20 mm, covering both typical fuselage/wing skin dimensions and associated features. The final PID predictions when subjected to prognosis at discrete time steps are validated with final experimental measures. Experimentally measured spring-in angles used for validation for cross-ply and unidirectional C-shaped part with 270° segments are reported in Wisnom et al.⁶² and Ersoy et al.²³ respectively. A C-shaped part of varying thickness, ranging from 1 to 4 mm, is fabricated with a stacking sequence of $[90^\circ/0^\circ]_{ns}$, and $[90^\circ]_{ns}$, where $n = 1, 2, 3, 4$. The part is manufactured on a carbon-epoxy mold with a negligible CTE. The pressure of 7 bars is applied throughout the MRCC curing cycle. The schematic profile of the material ply at the lamina level, along with the part made of lamina plies subject to different configurations, before and after the curing process, is illustrated in Figure 2.

The cured part sustains PIDs in form of spring-in angle, $\Delta\theta$, which is deemed to be a function of the volumetric free strains. Taking into consideration the constancy of material properties between the onset of gelation and vitrification and the abrupt shift in material properties during vitrification, an improved analytical solution³⁵ is introduced, given by,

$$\Delta\theta_k^i = - \left[(\varepsilon_R)_k^i + \mu_{ZR} \left((\varepsilon_Z)_k^i - C \right) \right] \left[\phi - \frac{e^{aR\phi} - e^{-aR\phi}}{Ra(e^{aR\phi} + e^{-aR\phi})} \right] + \phi \left[(\alpha_\theta^g)_k^i - (\alpha_R^g)_k^i \right] \Delta T, \quad (15)$$

where μ_{ZR} represents the out-of-plane Poisson's ratio, ε_Z represents the volumetric free strain in the length direction, ε_R represents the volumetric free strain in the through thickness direction, ΔT denotes the difference between vitrification and room temperatures, ϕ represents the radians of the curved part and C is the strain developed due to contact with the mold. In this context,

the variable R denotes the inner radius of the mold. The constant $a = \frac{10G_{\theta R}}{E_\theta b^2}$ introduces the influence of thickness b , the in-plane flexural modulus, E_θ and inter-laminate shear modulus $G_{\theta R}$ varying for different laminate configurations. This improved solution accurately captures the impact of deformation in the length direction when the material is in a rubbery state on spring-in.³⁵ The model considers strains in both the through-thickness and length directions for a more comprehensive analysis. This gives PIDs at a discrete time step, k , (i.e., $\Delta\theta_k^i : i = 1, 2, \dots, N_s$) corresponding to N_s predicted trajectories of Degree of Cure which is associated with a mean and a standard deviation.

For the prognosis of the PIDs, the relevant physical and mechanical properties of the AS4/8552 unidirectional material with fiber volume percentage of 57.4% are listed in Table 4. The effective properties that are missing are determined through micro-mechanical models, referring to the works.^{30,65} These models rely on semi-analytical and/or analytical expressions derived from the properties of the resin and fibers. The effective homogeneous properties for the cross-ply and unidirectional stacking sequence corresponding to different states are computed using the laminated plate theory, as listed in Table 5.^{35,62} The study⁶⁶ characterizes the effect of Degree of Cure evolution on the shrinkage-induced through-thickness strain for cross-ply specimens, which consequently modifies Equation (2) as follows:

$$\begin{cases} \varepsilon_R^f = \int_{t_{\text{gel}}}^{t_{\text{vitr}}} \alpha_R^f \left(\frac{\partial T}{\partial t} \right) dt + (2.156x^3 - 1.621x^2 - 2.697x + 0.928)\% \\ \varepsilon_R^g = \int_{t_{\text{vitr}}}^{t_{\text{final}}} \alpha_R^g \left(\frac{\partial T}{\partial t} \right) dt + (2.156x^3 - 1.621x^2 - 2.697x + 0.928)\% \end{cases} \quad (16)$$

For the case of cross-laminate plies configuration, lateral contraction in length direction is contained, allowing only through-thickness contraction to occur. Hence, the volumetric free strain is considered to be half of Equation (16) for the case of the unidirectional plies configuration, which can equally shrink in both through-thickness and length directions. The majority of shrinkage in AS4/8552 composites takes after end of first isothermal dwell, resulting in minimal movement of the mold, indicated by $C = 0$.

5 | RESULTS AND DISCUSSION

5.1 | Estimation results

Figure 3 highlights two important outcomes of the present analysis: (A) the sequentially updated mean on the

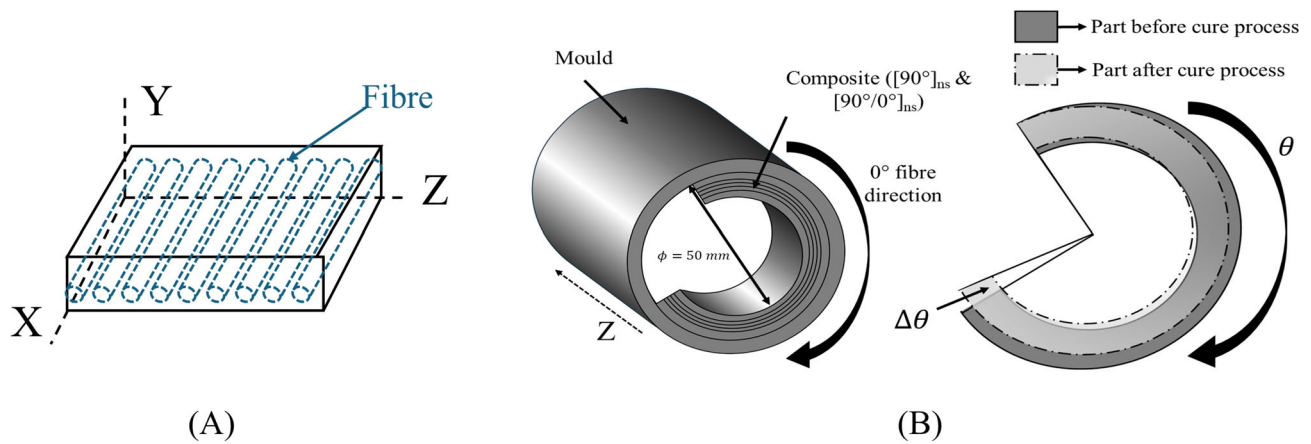


FIGURE 2 Schematic illustration of (A) material coordinate system (lamina level) and (B) C-shaped thermoset part before and after cure process (laminata level).

TABLE 4 Rubbery and glassy material properties of unidirectional at lamina level.⁶⁵

Properties	Uni-directional plies	
	Rubbery	Glassy
Longitudinal modulus, E_X (MPa)	132,200	135,000
Transversal modulus, E_Z (MPa)	165	9500
Through-thickness modulus, E_Y (MPa)	165	9500
In-plane shear modulus, G_{XZ} (MPa)	44.3	4900
Out-of-plane shear modulus, G_{XY} (MPa)	44.3	4900
Out-of-plane shear modulus, G_{ZY} (MPa)	41.6	3270
In-plane Poisson's ratio, μ_{ZY} (-)	0.346	0.300
Out-of-plane Poisson's ratio, μ_{XY} (-)	0.346	0.300
Out-of-plane Poisson's ratio, μ_{ZY} (-)	0.982	0.450
CTE in longitudinal direction, α_X ($1/^\circ\text{C}$)	0	0
CTE in transverse direction, α_Z ($1/^\circ\text{C}$)	0	0.326×10^{-4}
CTE in through thickness direction, α_Y ($1/^\circ\text{C}$)	0	0.326×10^{-4}

posterior PDF of the Degree of Cure along with the 95% confidence boundary (CB), and (B) the Ω^{sto} distribution at the initial time, gelation point, vitrification point, and final cure time. The initial joint distribution, $\Omega_{k=0}^{\text{sto}}$, is determined based on DSC characterization tests at various temperature rates, as discussed in Section 4.1. The

SIR PF approach updates and resamples the N_s particle weights, representing the posterior PDF of the Degree of Cure, at discrete time steps based on true measures. Subsequently, this adjustment influences the Ω^{sto} distribution accordingly.

After a few state updates, it is observed that the joint distribution clusters around a specific region in the case of MRCC. Specifically, the Ω^{sto} distribution converges around fixed values upon reaching the gelation point ($t = 7760 \text{ s}$). This can be visualized with help of root mean square errors (RMSE) metric for the Degree of Cure, given by,

$$\text{RMSE} = \sqrt{\frac{1}{t} \sum_{k=1}^t (x_{\text{mean},k} - x_{\text{true},k})^2}, \quad (17)$$

where $t = 204$ is the number of discrete time steps. Figure 4 represents the RMSE between the predicted Degree of Cure until cure completion and the true measures where the SIR procedure occurs. Beyond the gelation point, it is observed that the change in RMSE is negligible. This essentially means that beyond the gelation point, the sequentially updated parameters, Ω^{sto} , has the capability to model accurately the Degree of Cure and predict accurate cure transition points.

5.2 | Prognostic results

Figure 5A–D depicts the predicted trajectories of the Degree of Cure at the initial state, before, on, and after the occurrence of the gelation point. Each red line is the Degree of Cure trajectory predicted for one

TABLE 5 Equivalent homogenous rubbery and glassy material properties of cross-ply and unidirectional at laminate level.^{35,62}

Homogeneous properties	[90°/0°] _{ns}		[90°] _{ns}	
	Rubbery	Glassy	Rubbery	Glassy
In-plane flexural modulus, E_θ (MPa)	66,200	72,600	132,200	135,000
Through-thickness shear modulus, $G_{\theta R}$ (MPa)	43	4085	44.3	4900
Out-of-plane Poisson's ratio, μ_{RZ} (-)	0.830	0.438	0.982	0.450
CTE in hoop direction, α_θ (1/°C)	0	0.270×10^{-5}	0	0
CTE in thickness direction, α_R (1/°C)	0	0.452×10^{-4}	0	0.326×10^{-4}
CTE in length direction, α_Z (1/°C)	0	0.270×10^{-5}	0	0.326×10^{-4}

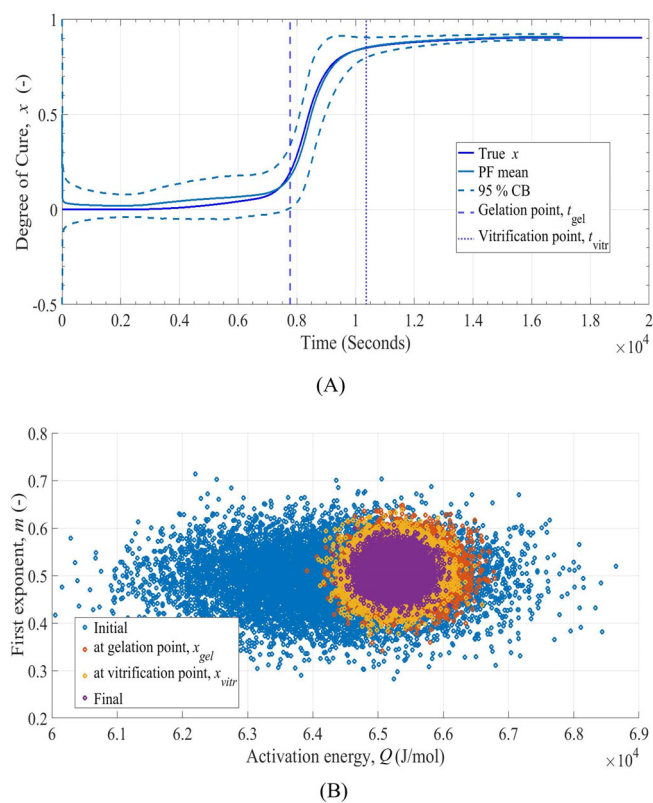


FIGURE 3 Particle filters (PF) diagnostic results showing (A) the sequentially updated mean on the posterior Probability Density Function (PDF) along with the 95% CB and (B) Ω^{sto} joint distribution at discrete time steps.

posterior sample of Degree of Cure vector. The black dashed and dotted lines represent the estimate of the PDF for the occurrences of gelation and vitrification points corresponding to the predicted Degree of Cure trajectories. The uncertainty linked to sequential Degree of Cure updates diminishes upon reaching the gelation point. The accurate prediction of the vitrification point, lasting until the completion of the manufacturing process, is credited to the improved reliability of the Ω^{sto} distribution transitioning to the

rubbery state. This can be observed as the estimate of the PDF moves toward the true occurrence of the vitrification point with an updated Ω^{sto} distribution from estimation results.

Subsequently, predictions of PIDs are generated based on gelation and vitrification points' PDF estimates from Degree of Cure trajectories at discrete time steps. Figure 6A,B depicts the PF PID prognosis for a C-shaped part with a thickness of 4 mm in terms of spring-in angle, $\Delta\theta$, with using both unidirectional and cross-ply configurations. The prognosis is conducted over 204 discrete time steps, utilizing N_s trajectories of Degree of Cure at each time step. The PID predictions before the gelation point are poor due to occurrence incorrect transition points. During the initial time steps, refer to Figure 5A, the Ω^{sto} distribution remains uncorrelated, resulting in dense trajectories of the Degree of Cure evolution. The dense trajectories are associated with the estimate of the PDF for the occurrences of gelation and vitrification points spread over large intervals of time steps in the cure process. The global mean of the estimate of PDF for the gelation and vitrification points lies after true t_{gel} and before true t_{vitr} respectively. This leads to swift transitions between rubbery and glassy states, with the transition to the glassy state occurring during the second heating ramp within the MRCC. This leads to additional thermoelastic contribution to volumetric free strains in glassy state, negating the contribution from shrinkage incurred in the rubbery state. Consequently, this results in less process-induced spring-in.

Meanwhile, in subsequent discrete time steps before gelation, the trajectories of the Degree of Cure evolution start to narrow with the update of the Ω^{sto} distribution from estimation results. This can be seen in Figure 5B. While the estimate of the PDF for the occurrences of t_{gel} coincides with the true t_{gel} , the estimate of the PDF for the occurrences of t_{vitr} spreads over large intervals of time steps corresponding to the second dwell and cooling cycle of the cure process. For trajectories where t_{vitr} occurs during the cool-down ramp, results in relatively less overall

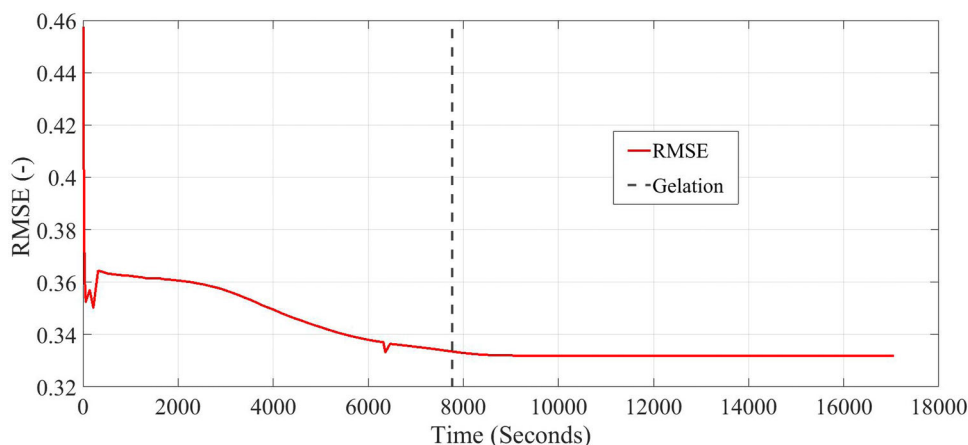


FIGURE 4 Particle filters (PF) performance with updated Ω^{sto} at discrete time steps.

volumetric free strain during cool-down, leading to less spring-in than the actual measures.

Notably, after the gelation point (also the end of the first isothermal dwell in MRCC), it is observed that the projected final PID predictions align with the experimental measures of 0.63° and 0.96° for the case of unidirectional plies and cross-ply configuration, respectively.^{23,62} The mean estimate of the PDF for the occurrence of the vitrification point progressively converges toward the actual true vitrification point position. Consequently, higher confidence levels can be achieved in the PIDs predictions when intentional temperature changes are triggered upon reaching the time corresponding to the gelation point in thermal loading conditions. This confidence is gained through the update of the Ω^{sto} distribution post-gelation, which inherently accounts for stochasticity associated with thermal loading uncertainty.

5.3 | PF performance under varying thermal loading conditions

The temperature of the part is strongly affected by both the convection coefficient and the Degree of Cure, as demonstrated in Figure 7 for a case involving the MRCC with two isothermal dwells. The study incorporates a C-shaped part made of cross-ply with a thickness of 15 mm. The values of thermochemical properties, namely density, thermal conductivity, and specific heat, are 1594 kg/m^3 , $1.170 \text{ W/m}^\circ\text{C}$, and $1289 \text{ J/kg}^\circ\text{C}$, respectively.^{31,61,67}

The autoclave convection coefficient, ranging between 20 and $100 \text{ W/m}^2\text{C}$, is significantly influenced by the inherent variability in the autoclave process, impacting the temperature of the part. The FE-based heat transfer analyses predict a temperature profile range that the part follows, considering the convective boundary condition in the part thickness direction.²⁷ The red zone

illustrates the associated standard deviations corresponding to the exotherm lag following the conclusion of the initial isothermal dwell in MRCC.

The validation of PF prognosis performance is conducted using state-of-the-art numerical analysis with an autoclave boundary condition. The detailed viscoelastic constitutive model formulation³³ provided in Appendix, is taken into account. The FE model as illustrated in Figure 8 considers the pressure cycle applied to the free surface of the C-shaped part. The 3D geometrical model is created by extruding and meshing in the thickness direction of the defined shell geometry. Prior to extrusion, the materials, thickness, and orientations of plies were defined. The draping modeling is performed with the help of Simulayt Composite Modeler within ABAQUS. In the 3D model, the part is represented by 248,400 hexahedral C3D8 elements with linear geometrical order and assigned local orientations. The mold, made of carbon-epoxy with a negligible thermal expansion coefficient, is modeled as a rigid part, using 10,948 quadrilateral R3D4 elements with linear geometrical order.

The purpose of the imposed boundary condition in the numerical model is to closely replicate the experimental conditions, where pressure holds the part against the mold, preventing the curved section from closing freely. The nominal production temperature and pressure cycles are applied accordingly during the curing step. Finally, in the demoulding step, the pressure and contact with the mold are removed to predict distortions. The mechanical and thermo-chemical properties used for the numerical analysis are extracted from Table 4. The mean values of the sequentially estimated Ω^{sto} , along with other deterministic cure model parameters, Ω^{det} , are considered for the numerical simulation.

The PF predictions are then compared with the FE-based viscoelastic constitutive model, as shown in Figure 9. The final predictions obtained through the PF prognostic approach show excellent agreement with the

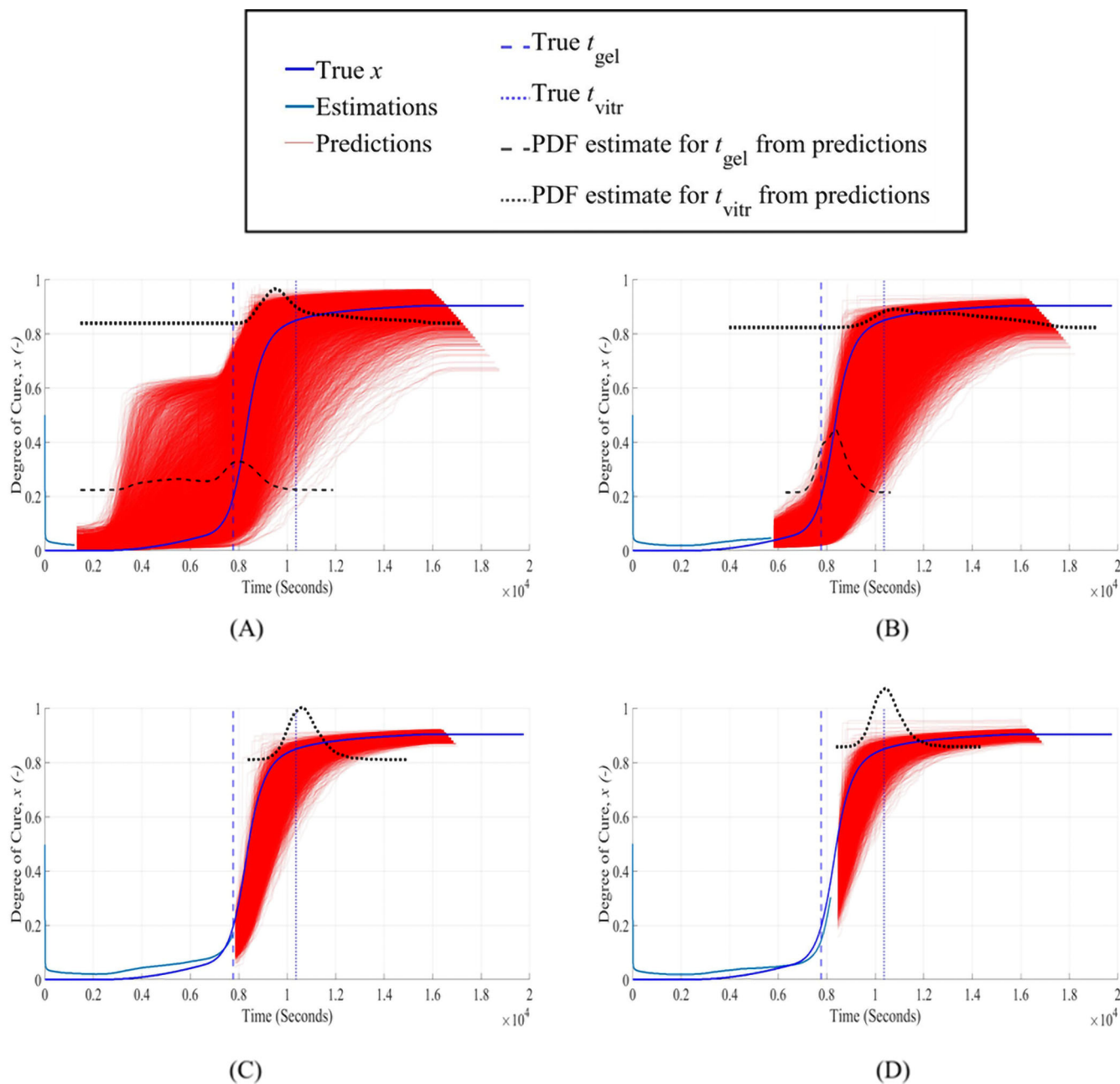


FIGURE 5 Future Degree of Cure predictions (A) at the initial state, (B) before, (C) on, and (D) after the occurrence of the gelation point.

state-of-the-art constitutive model right after the gelation point. It is observed that the case where the cure profile reaches its upper limit are associated with higher PIDs, and vice versa. This occurs because faster heat ramps from gelation points lead to a quicker transition to the glassy state, resulting in higher internal residual stress and volumetric free strains associated with elevated mechanical properties. This can be observed in Figure 10 through the comparison of overall displacements from the FE-based constitutive model with three different thermal loading condition scenarios.

In terms of computational efficiency, the FE-based constitutive model, run using ABAQUS explicit on a personal computer equipped with an Intel Core i5-10300H CPU boasting eight processors, on average requires 405 min for computation. The FE-based analysis is carried out with a fixed time increment of 10 s, corresponding to the same time increment used within the PF implementation. In contrast, the converged PF prognostic model utilizing 8000 particles, only takes between 8 and 10 s to predict the PIDs at every discrete time step. This significantly enhanced computational

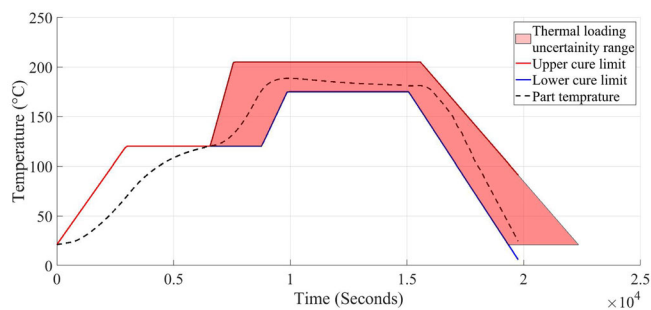
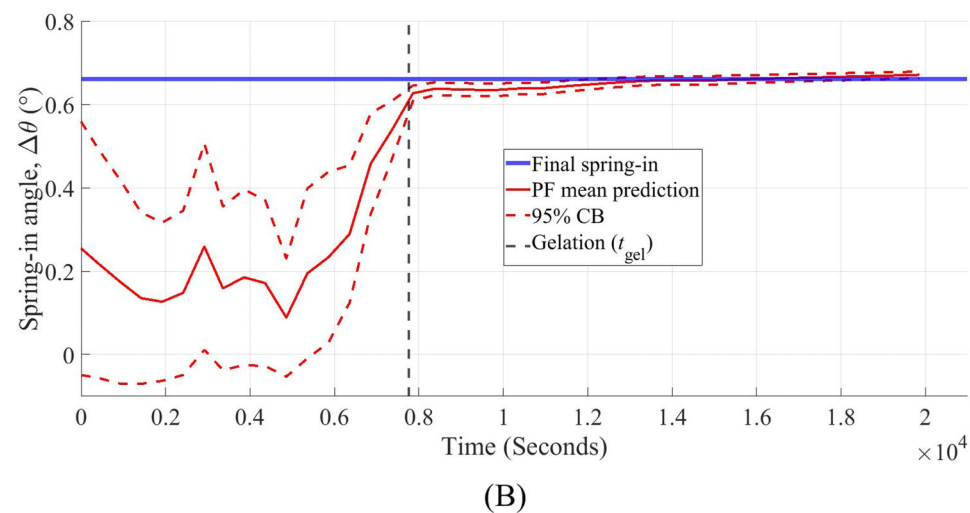
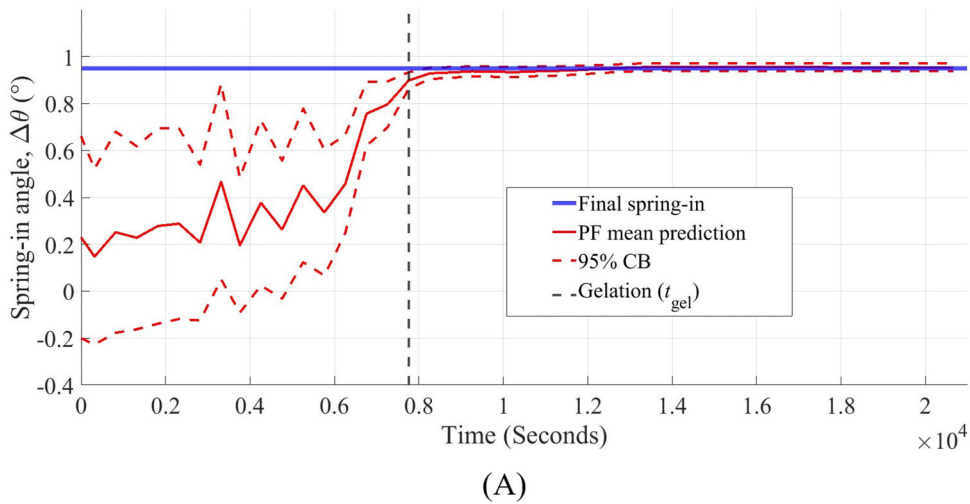


FIGURE 7 Actual part temperature (with convection coefficient of $40 \text{ W/m}^2\text{C}$) in thickness direction along with its associated upper and lower limits.

capability proves invaluable, especially for active manufacturing control systems. It becomes particularly useful when dealing with unknown or stochastic convective boundary conditions, showcasing the practicality and adaptability of this approach in complex manufacturing scenarios.

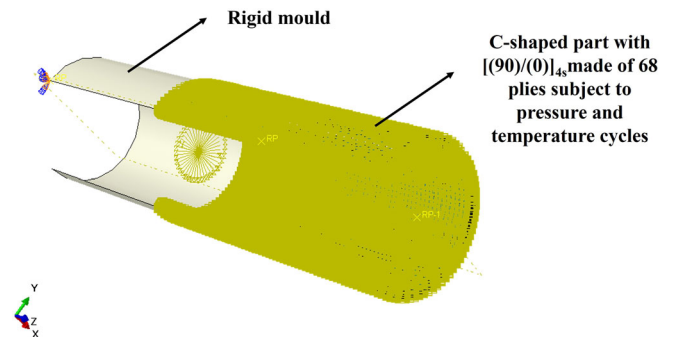


FIGURE 8 Finite element model for C-shaped parts with a thickness of 15 mm, made of cross-ply, along with its associated cure boundary conditions.

6 | CONCLUSION

There is a greater need for active manufacturing control, involving the integration of real-time monitoring, data analyses, and predictive modeling approaches to improve the manufacturing process. Hence, models leveraging

FIGURE 9 Forecasting of process-induced deformations using estimated model parameters at discrete time steps for the upper and lower cure cycle limits.

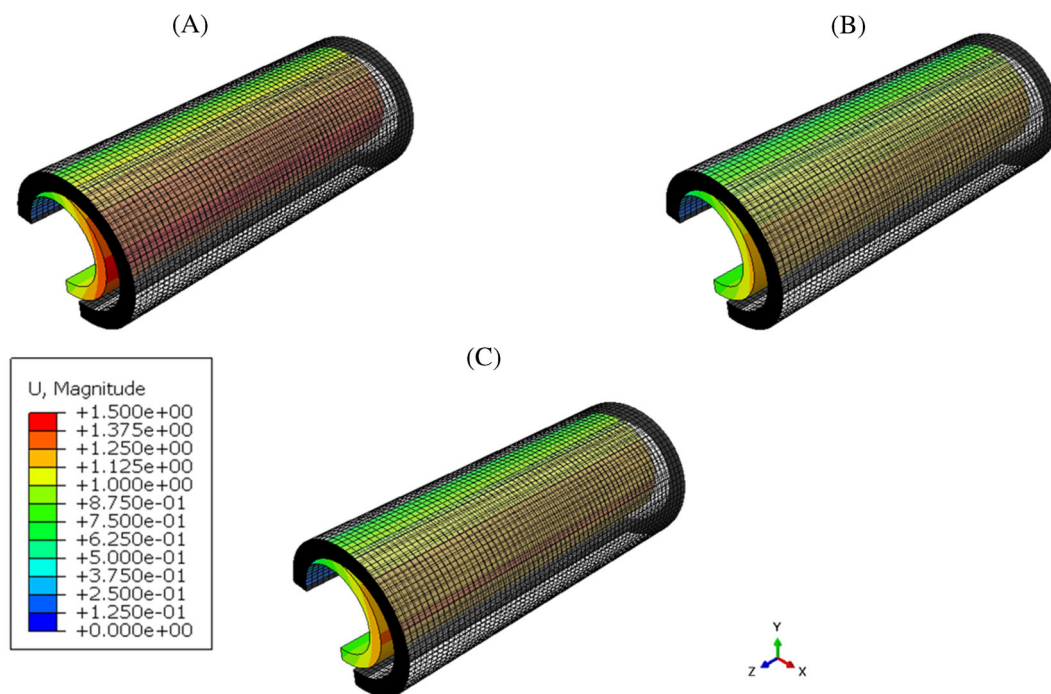
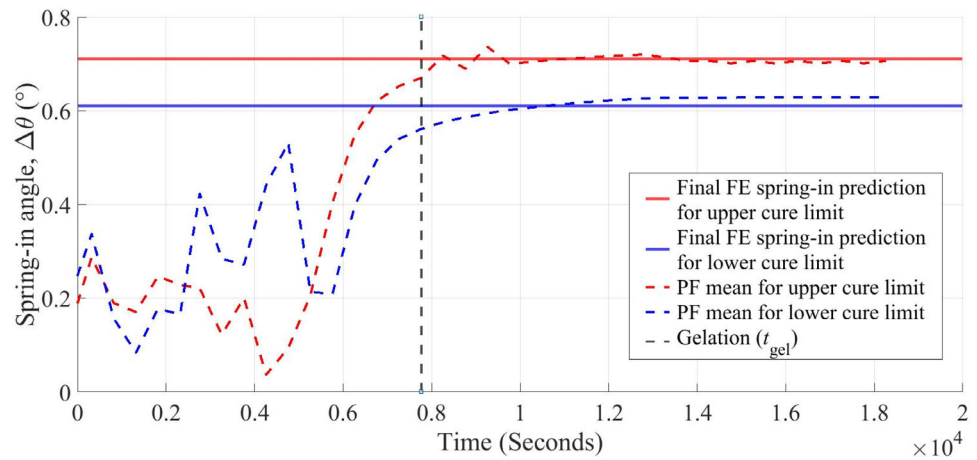


FIGURE 10 Comparison of overall displacement for the cure cycle with the finite element-based constitutive model corresponding to (A) upper limit, (B) lower limit, and (C) actual part temperature (scaling deformation factor = 5.0).

material data, prior knowledge, and measurements can be used to forecast potential defects that may arise during manufacturing.

The study incorporates the use of PF which can be used for estimation model parameters associated with Degree of Cure and forecasting the Degree of Cure with change in thermal loading conditions. This is done by propagating a set of particles through the time frames, representing the Degree of Cure, and updating their associated weights based on measured characterization DSC tests. The DSC data provide valuable information about the cure process associated parameters. The data is regarded as prior knowledge is integrated into the

methodology to enhance the model parameters estimations, thereby improving the accuracy of Degree of Cure estimates. The methodology is integrated with the thermoset part's actual cure profile during the curing process to make arcuate PID predictions based on prognosis of Degree of Cure. This is because the part's temperature is different to the oven's temperature because of various intrinsic factors. The conclusion from the study are as follows:

- Diffusion cure-kinetics parameters, especially the activation energy and first exponent, have a significant influence on Degree of Cure and must be treated

stochastically to address uncertainties related to thermal loading conditions.

- The framework facilitates the accurate prediction of PIDs beyond the gelation point for cases involving C-shaped parts made of AS4/8552 prepregs. This is observed by the alignment of the estimates of PDF corresponding to the vitrification point with the N_s trajectories of Degree of Cure after the gelation point occurrence.
- The framework effectively defines PID variations when dealing with thick composite parts experiencing temperature fluctuations. The inherent stochasticity of the activation energy and first exponent after gelation accounts for uncertainties in thermal loading conditions.

The key finding of the study is that the uncertainty related to sequential updates of the Degree of Cure diminishes when reaching the gelation point, which corresponds to the end of the first isothermal dwell in the MRCC. This is confirmed by the observed convergence of PID taking place right after the end of the first isothermal dwell corresponding to MRCC. This converged PF prognosis capability can be integrated with evolutionary algorithms to perform multi-objective optimization for cure cycle design beyond the first isothermal dwell, aiming to minimize total cure time and PIDs. Therefore, the combination of multi-objective optimization with stochastic PF simulations can be implemented for real-time optimization of the curing cycle, enabling online monitoring and control over the curing process. In future developments, the model could be expanded to encompass different materials and geometries. Overall, utilizing online diagnosis and prognosis models in active thermoset manufacturing allows for a data-driven and proactive approach, leading to enhanced process reliability, quality assurance, and cost-effectiveness.

ACKNOWLEDGMENTS

This project has received funding from the European Union's Horizon 2020 research and innovation programme under the Marie Skłodowska-Curie grant agreement no. 859957. Portions of this work were done while the author, Olivier Pierard was affiliated with Cenaero Research Center.

DATA AVAILABILITY STATEMENT

Data sharing not applicable to this article as no datasets were generated during the current study.

ORCID

Aravind Balaji  <https://orcid.org/0009-0005-1893-5685>

REFERENCES

1. Advani SG, Sozer E. *Process Modeling in Composites Manufacturing*. 2nd ed. CRC Press; 2010.
2. Svanberg J. Predictions of Manufacturing Induced Shape Distortions: High Performance Thermoset Composites. PhD thesis. Luleå tekniska universitet. 2002.
3. Callister WD, Rethwisch DG. *Materials Science and Engineering: an Introduction*. 8th ed. Wiley; 2007.
4. Parlevliet P, Bersee HEN, Beukers A. Residual stresses in thermoplastic composites—a study of the literature—part I: formation of residual stresses. *Compos A: Appl Sci Manuf*. 2006;37(11):1847-1857. doi:10.1016/j.compositesa.2005.12.025
5. Zobeiry N, Poursartip A. The origins of residual stress and its evaluation in composite materials. In: Beaumont PWR, Soutis C, Hodzic A, eds. *Structural Integrity and Durability of Advanced Composites*. Woodhead Publishing Series in Composites Science and Engineering. Woodhead Publishing; 2015:43-72. doi:10.1016/b978-0-08-100137-0.00003-1
6. Lange J, Toll S, Månson JE, Hult A. Residual stress build-up in thermoset films cured above their ultimate glass transition temperature. *Polymer*. 1995;36(16):3135-3141. doi:10.1016/0032-3861(95)97876-h
7. Ersoy N, Potter KD, Wisnom MR, Clegg MJ. Development of spring-in angle during cure of a thermosetting composite. *Compos A: Appl Sci Manuf*. 2005;36(12):1700-1706. doi:10.1016/j.compositesa.2005.02.013
8. Seers B, Tomlinson R, Fairclough P. Residual stress in fiber reinforced thermosetting composites: a review of measurement techniques. *Polym Compos*. 2021;42:1631-1647. doi:10.1002/pc.25934
9. Twigg G, Poursartip A, Fernlund G. Tool-part interaction in composites processing. Part I: experimental investigation and analytical model. *Compos A: Appl Sci Manuf*. 2004;35(1):121-133. doi:10.1016/s1359-835x(03)00131-3
10. Garstka T. Separation of Process Induced Distortions in Curved Composite Laminates. PhD thesis. The University of Bristol. 2005.
11. Parmentier A, Dumas D. Influence of the tool-part frictional interaction on the cure-induced deformations in thermoset-based composite parts. *Proceedings of the 21th International Conference on Composite Materials*. Chinese Society for Composite Materials; 2017.
12. Nawab Y, Sonnenfeld C, Saouab A, Agogué R, Beauchêne P. Characterisation and modelling of thermal expansion coefficient of woven carbon/epoxy composite and its application to the determination of spring-in. *J Compos Mater*. 2016;51(11):1527-1538. doi:10.1177/0021998316661404
13. Kappel E, Stefaniak D, Hühne C. Process distortions in prepreg manufacturing – an experimental study on CFRP L-profiles. *Compos Struct*. 2013;106:615-625. doi:10.1016/j.compstruct.2013.07.020
14. Wang B, Fan S, Chen J, Yang W, Liu W, Li Y. A review on prediction and control of curing process-induced deformation of continuous fiber-reinforced thermosetting composite structures. *Compos A: Appl Sci Manuf*. 2023;165:107321. doi:10.1016/j.compositesa.2022.107321
15. Joosten M, Agius S, Hilditch T, Wang CH. Effect of residual stress on the matrix fatigue cracking of rapidly cured epoxy/anhydride composites. *Compos A: Appl Sci Manuf*. 2017;101:521-528. doi:10.1016/j.compositesa.2017.07.007

16. Takagaki K, Minakuchi S, Takeda N. Process-induced strain and distortion in curved composites. Part I: development of fiber-optic strain monitoring technique and analytical methods. *Compos A: Appl Sci Manuf.* 2017;103:236-251. doi:10.1016/j.compositesa.2017.09.020
17. Nelson RH, Cairns DS. Prediction of dimensional changes in composite laminates during cure. *Proceedings of the 34th International SAMPE Symposium and Exhibition.* Society for the Advancement of Material and Process Engineering; 1989:2397-2410.
18. Hamamoto A. Curing of L-shaped composite parts. *Proceedings of International Symposium on Composite Materials and Structures.* Technomic Publishing Co, Inc; 1986:1092-1097.
19. Radford DW, Rennick TS. Separating sources of manufacturing distortion in laminated composites. *J Reinf Plast Compos.* 2000; 19(8):621-641. doi:10.1177/073168440001900802
20. Stair S, Jack DA. Comparison of experimental and modeling results for cure induced curvature of a carbon fiber laminate. *Polym Compos.* 2017;38:2488-2500. doi:10.1002/pc.23838
21. White SR, Hahn HT. Mechanical property and residual stress development during cure of a graphite/BMI composite. *Polym Eng Sci.* 1990;30:1465-1473. doi:10.1002/pen.760302207
22. Kappel E. Forced-interaction and spring-in—relevant initiators of process-induced distortions in composite manufacturing. *Compos Struct.* 2016;140:217-229. doi:10.1016/j.compstruct.2016.01.016
23. Ersoy N, Garstka T, Potter KD, Wisnom MR, Porter D, Stringer G. Modelling of the spring-in phenomenon in curved parts made of a thermosetting composite. *Compos A: Appl Sci Manuf.* 2010;41(3):410-418. doi:10.1016/j.compositesa.2009.11.008
24. Ding A, Li S, Sun J, Wang J, Zu L. A comparison of process-induced residual stresses and distortions in composite structures with different constitutive laws. *J Reinf Plast Compos.* 2016;35(10):807-823. doi:10.1177/0731684416629764
25. White SR, Hahn HT. Process modeling of composite materials: residual stress development during cure. Part I. Model formulation. *J Compos Mater.* 1992;26(16):2402-2422. doi:10.1177/002199839202601604
26. Kim YK, White SR. Stress relaxation behavior of 3501-6 epoxy resin during cure. *Polym Eng Sci.* 1996;36(23):2852-2862. doi:10.1002/pen.10686
27. Kim YK, White SR. Viscoelastic analysis of processing-induced residual stresses in thick composite laminates. *Mech Adv Mater Struct.* 1997;4(4):361-387. doi:10.1080/10759419708945889
28. Prasatya P, McKenna GB, Simon SL. A viscoelastic model for predicting isotropic residual stresses in thermosetting materials: effects of processing parameters. *J Compos Mater.* 2001; 35(10):826-848. doi:10.1177/a037322
29. Ding A, Li S, Wang J, Zu L. A three-dimensional thermo-viscoelastic analysis of process-induced residual stress in composite laminates. *Compos Struct.* 2015;129:60-69. doi:10.1016/j.compstruct.2015.03.034
30. Bogetti TA, Gillespie JW. Process-induced stress and deformation in thick-section thermoset composite laminates. *J Compos Mater.* 1992;26(5):626-660. doi:10.1177/002199839202600502
31. Johnston AA, Vaziri R, Poursartip A. A plane strain model for process-induced deformation of laminated composite structures. *J Compos Mater.* 2001;35(16):1435-1469. doi:10.1106/YXEA-5MH9-76J5-BACK
32. Zobeiry N, Vaziri R, Poursartip A. Computationally efficient pseudo-viscoelastic models for evaluation of residual stresses in thermoset polymer composites during cure. *Compos A: Appl Sci Manuf.* 2010;41(2):247-256. doi:10.1016/j.compositesa.2009.10.009
33. Svanberg J, Holmberg JA. Prediction of shape distortions part I. FE-implementation of a path dependent constitutive model. *Compos A: Appl Sci Manuf.* 2004;35(6):711-721. doi:10.1016/j.compositesa.2004.02.005
34. Galińska A. Compensation of process-induced deformations of double-curved carbon–epoxy composite elements. *Polym Compos.* 2019;40:3666-3677. doi:10.1002/pc.25229
35. Ding A, Li S, Wang J, Ni A. A new analytical solution for spring-in of curved composite parts. *Compos Sci Technol.* 2017; 142:30-40. doi:10.1016/j.compscitech.2017.01.024
36. Ding A, Wang J, Li S. Understanding process-induced spring-in of L-shaped composite parts using analytical solution. *Compos Struct.* 2020;250:112629. doi:10.1016/j.compstruct.2020.112629
37. Ding A, Wang J, Ni A, Li S. A new analytical solution for cure-induced spring-in of L-shaped composite parts. *Compos Sci Technol.* 2019;171:1-12. doi:10.1016/j.compscitech.2018.12.004
38. Mesogitis TS, Skordos AA, Long AC. Uncertainty in the manufacturing of fibrous thermosetting composites: a review. *Compos A: Appl Sci Manuf.* 2014;57:67-75. doi:10.1016/j.compositesa.2013.11.004
39. Mesogitis TS, Skordos AA, Long AC. Stochastic simulation of the influence of fibre path variability on the formation of residual stress and shape distortion. *Polym Compos.* 2017;38:2642-2652. doi:10.1002/pc.23856
40. Tifkitsis K, Mesogitis TS, Struzziero G, Skordos AA. Stochastic multi-objective optimisation of the cure process of thick laminates. *Compos A: Appl Sci Manuf.* 2018;112:383-394. doi:10.1016/j.compositesa.2018.06.015
41. Struzziero G, Skordos AA. Multi-objective optimisation of the cure of thick components. *Compos A: Appl Sci Manuf.* 2017;93: 126-136. doi:10.1016/j.compositesa.2016.11.014
42. Mesogitis T, Skordos AA, Long AC. Stochastic heat transfer simulation of the cure of advanced composites. *J Compos Mater.* 2016;50(21):2971-2986. doi:10.1177/0021998315615200
43. Padmanabhan SK, Pitchumani R. Stochastic analysis of isothermal cure of resin systems. *Polym Compos.* 1999;20(1):72-85. doi:10.1002/pc.10336
44. Mesogitis T, Skordos AA, Long AC. Stochastic simulation of the influence of cure kinetics uncertainty on composites cure. *Compos Sci Technol.* 2015;110:145-151. doi:10.1016/j.compscitech.2015.02.009
45. Zobeiry N, Poursartip A. Theory-Guided machine learning for process simulation of advanced composites. arXiv (Cornell University). 2021. doi:10.48550/arXiv.2103.16010
46. Carlone P, Aleksendrić D, Ćirović V, Palazzo GS. Meta-modeling of the curing process of thermoset matrix composites by means of a FEM–ANN approach. *Compos Part B: Eng.* 2014; 67:441-448. doi:10.1016/j.compositesb.2014.08.022
47. Luo L, Zhang B, Zhang G, et al. Rapid prediction and inverse design of distortion behaviors of composite materials using artificial neural networks. *Polym Adv Technol.* 2021;32:1049-1060. doi:10.1002/pat.5152
48. Hou J, You B, Xu J, Wang T. Prediction of curing process for thermosetting prepreg compression molding process based on

- machine learning. *Polym Compos.* 2022;43(3):1749-1762. doi:10.1002/pc.26494
49. Johnston A, Hubert P, Nelson K, Poursartip A, Fernlund G. A sensitivity analysis of modelling predictions of the warpage of a composite structure. *Proceedings of the 43rd International SAMPE Symposium and Exhibition.* Society for the Advancement of Material and Process Engineering; 1998:629-640.
 50. Zhou K, Enos R, Zhang D, Tang J. Uncertainty analysis of curing-induced dimensional variability of composite structures utilizing physics-guided gaussian process meta-modeling. *Compos Struct.* 2022;280:114816. doi:10.1016/j.compstruct.2021.114816
 51. Çınar K, Öztürk UE, Ersoy N, Wisnom MR. Modelling manufacturing deformations in corner sections made of composite materials. *J Compos Mater.* 2013;48(7):799-813. doi:10.1177/0021998313477896
 52. Hui X, Ye X, Zhang W, Zhang W. Multiscale collaborative optimization for the thermochemical and thermomechanical cure process during composite manufacture. *Compos Sci Technol.* 2022;224:109455. doi:10.1016/j.compscitech.2022.109455
 53. Zhang W, Ye X, Hui X, Zhang W. A multi-dwell temperature profile design for the cure of thick CFRP composite laminates. *Int J Adv Manuf Technol.* 2021;117:1133-1146. doi:10.1007/s00170-021-07765-1
 54. Cole KP, Hechler JJ, Noël D. A new approach to modeling the cure kinetics of epoxy/amine thermosetting resins. 2. Application to a typical system based on bis[4-(diglycidylamino)phenyl]methane and bis(4-aminophenyl) sulfone. *Macromolecules.* 1991;24(11):3098-3110. doi:10.1021/ma00011a012
 55. Doucet A, de Freitas N, Gordon N. An introduction to sequential Monte Carlo methods. In: Doucet A, de Freitas N, Gordon N, eds. *Sequential Monte Carlo Methods in Practice. Statistics for Engineering and Information Science.* Springer; 2001. doi:10.1007/978-1-4757-3437-9_1
 56. Gordon N, Salmond D, Smith AFM. Novel approach to nonlinear/non-gaussian Bayesian state estimation. *IEE Proc.* 1993; 140(2):107. doi:10.1049/ip-f-2.1993.0015
 57. Arulampalam MS, Maskell S, Gordon N, Clapp T. A tutorial on particle filters for online nonlinear/non-gaussian Bayesian tracking. *IEEE Trans Signal Process.* 2002;50(2):174-188. doi:10.1109/78.978374
 58. Jouin M, Gouriveau R, Hissel D, Pera M, Zerhouni N. Particle filter-based prognostics: review, discussion and perspectives. *Mech Syst Signal Process.* 2016;72-73:2-31. doi:10.1016/j.ymssp.2015.11.008
 59. Stütz H, Illers KH, Mertes J. A generalized theory for the glass transition temperature of crosslinked and uncrosslinked polymers. *J Polym Sci Part B: Polym Phys.* 1990;28(9):1483-1498. doi:10.1002/polb.1990.090280906
 60. Kappel E. An engineering approach for prepreg characterization. *Compos C: Open Access.* 2021;4:100083. doi:10.1016/j.jcomc.2020.100083
 61. Hexply 8552 product data sheet. Mid-toughened, high strength, damage-resistant, structural epoxy matrix. <https://www.hexcel.com/> 2016. Accessed March 16, 2022.
 62. Wisnom MR, Potter KD, Ersoy N. Shear-lag analysis of the effect of thickness on spring-in of curved composites. *J Compos Mater.* 2006;41(11):1311-1324. doi:10.1177/0021998306068072
 63. Dykeman D. Minimizing Uncertainty in Cure Modeling for Composites Manufacturing. PhD thesis. The University of British Columbia, Vancouver. 2008.
 64. Liu J, West M. Combined parameter and state estimation in simulation-based filtering. In: Doucet A, de Freitas N, Gordon N, eds. *Sequential Monte Carlo Methods in Practice. Statistics for Engineering and Information Science.* Springer; 2001. doi:10.1007/978-1-4757-3437-9_10
 65. Ersoy N, Garstka T, Potter K, et al. Development of the properties of a carbon fiber reinforced thermosetting composite through cure. *Compos A: Appl Sci Manuf.* 2010;41(3):401-409. doi:10.1016/j.compositesa.2009.11.007
 66. Garstka T, Ersoy N, Potter KD, Wisnom MR. In situ measurements of through-the-thickness strains during processing of AS4/8552 composite. *Compos A: Appl Sci Manuf.* 2007;38(12): 2517-2526. doi:10.1016/j.compositesa.2007.07.018
 67. Farmer JD, Covert EE. Thermal conductivity of a thermosetting advanced composite during its cure. *J Thermophys Heat Transf.* 1996;10(3):467-475. doi:10.2514/3.812
 68. Zocher MA, Groves SE, Allen DH. A three-dimensional finite element formulation for thermoviscoelastic orthotropic media. *Int J Numer Methods Eng.* 1997;40(12):2267-2288. doi:10.1002/(sici)1097-0207(19970630)40:12

How to cite this article: Balaji A, Dumas D, Pierard O, Sbarufatti C, Cadini F. Particle filter-based prognostics for composite curing process. *Polym Compos.* 2024;45(14):12913-12931. doi:10.1002/pc.28677

APPENDIX A

A.1 | Maxwell's viscoelastic constitutive model

The instantaneous relaxation modulus corresponding to the Maxwell's element with a spring and dashpot system within the viscoelastic model of the partially cured resin depends on the cure process variables (x and T_g). The viscoelastic model of the partially cured resin, depends on the reduced time associated with the spring and dashpot, denoted by ψ and ψ' , respectively. The thermo-viscoelastic behavior for anisotropic and thermo-chemo-rheological materials is expressed in integral form, where it is a function of the instantaneous relaxation modulus, C . The equation is given as:

$$\sigma(t) = C\epsilon + \int_0^t \delta C(\psi - \psi') \frac{\partial(\epsilon^{mech} - \epsilon)}{\partial \tau} \partial \tau, \quad (A1)$$

where C represents the linear elastic Hooke tensor, δC is the independent relaxation function of N Maxwell

elements and $\boldsymbol{\epsilon}^{\text{mech}}$ denotes the mechanical non volumetric free strain. The dependence of ψ and ψ' on cure process variables is established using a shift factor, a_T , in the constitutive model given by:

$$\psi = \int_0^t \frac{1}{a_T} dt'; \psi' = \int_0^t \frac{1}{a_T} dt'. \quad (\text{A2})$$

The generalized Maxwell's model with N elements in parallel with a free spring, provides the relaxation Hooke's tensor as follows:

$$\mathbf{C} = \begin{cases} 0, \forall x < x_{\text{gel}} \\ \mathbf{C}_{\infty} + \sum_{n=1}^N \mathbf{C}_n e^{(-t)\rho^n}, \forall x \geq x_{\text{gel}} \end{cases}, \quad (\text{A3})$$

where \mathbf{C}_{∞} is the fully relaxed modulus of uncured resin, \mathbf{C}_n is the spring constant, ρ^n are the relaxation times, with n denoting the Maxwell element.

The shift factor, a_T is assumed to be a function that approaches zero in the rubbery state and infinity in the glassy state. A variable γ is incorporated to establish the functional approximation of a_T , as expressed by:

$$a_T = \lim_{\gamma \rightarrow 0} \begin{cases} \gamma, \forall T \geq T_g(x) \\ \frac{1}{\gamma}, \forall T < T_g(x). \end{cases} \quad (\text{A4})$$

This assumption governs the behavior of the Hooke tensor: in the rubbery state, \mathbf{C}_r is denoted as the fully relaxed Hooke tensor, \mathbf{C}_{∞} while in the glassy state, \mathbf{C}_g is represented as $\left(\mathbf{C}_{\infty} + \sum_{n=1}^N \mathbf{C}_n\right)$. The Equation (A1-A4) are simplified, and the stress field is written as,

$$\boldsymbol{\sigma} = \begin{cases} \mathbf{C}_r(\boldsymbol{\epsilon}^{\text{mech}} - \boldsymbol{\epsilon}), \forall T \geq T_g(x) \\ \mathbf{C}_g(\boldsymbol{\epsilon}^{\text{mech}} - \boldsymbol{\epsilon}) - (\mathbf{C}_g - \mathbf{C}_r)(\boldsymbol{\epsilon}^{\text{mech}} - \boldsymbol{\epsilon})|_{t=t_{\text{vitr}}}, \forall T < T_g(x). \end{cases} \quad (\text{A5})$$

An incremental formulation, with the rate dependence replaced by a path dependence on the cure process variables, is performed based on Equations (A1)–(A4).³³ The incremental stress state is incorporated into the FE-tool following the approach outlined.⁶⁸ The stress increment upon simplification corresponding to a time step, Δt , is given by,

$$\Delta \boldsymbol{\sigma} = \begin{cases} \mathbf{C}_r \Delta(\boldsymbol{\epsilon}^{\text{mech}} - \boldsymbol{\epsilon}) - \mathbf{S}(t), \forall T \geq T_g(x) \\ \mathbf{C}_g \Delta(\boldsymbol{\epsilon}^{\text{mech}} - \boldsymbol{\epsilon}), \forall T < T_g(x) \end{cases}, \quad (\text{A6})$$

where \mathbf{S} represents the internal residual stress field, which evolves based on the loading history and is calculated as,

$$\mathbf{S}(t + \Delta t) = \begin{cases} 0, \forall T \geq T_g(x) \\ \mathbf{S}(t) + (\mathbf{C}_g - \mathbf{C}_r) \Delta(\boldsymbol{\epsilon}^{\text{mech}} - \boldsymbol{\epsilon}), \forall T < T_g(x). \end{cases} \quad (\text{A7})$$

The state variable, denoted as \mathbf{S} , is calculated based on the boundary conditions and the evolution of cure-state variables. In the rubbery and viscous states, the material is assumed to be fully relaxed, resulting in \mathbf{S} being assigned a value of zero. In contrast, during the glassy state, an internal stress state is progressively accumulated. This internal residual stress is ultimately released upon the completion of the curing process, resulting in distorted shapes.